We are IntechOpen,
the world's leading publisher of
Open Access books
Built by scientists, for scientists

6,900
Open access books available

186,000
International authors and editors

200M
Downloads

Our authors are among the

154
Countries delivered to

TOP 1%
most cited scientists

12.2%
Contributors from top 500 universities

CLARIVATE ANALYTICS
BOOK CITATION INDEX
INDEXED

WEB OF SCIENCE™

Selection of our books indexed in the Book Citation Index
in Web of Science™ Core Collection (BKCI)

Interested in publishing with us?
Contact book.department@intechopen.com

Numbers displayed above are based on latest data collected.
For more information visit www.intechopen.com

Chapter

Anisotropic Mechanical Properties of 2-D Materials

Qiang Li

Abstract

While prior reviews and research articles focused on the various synthetic routes and microstructural controls of 2D nanomaterials as well as their functional applications, this chapter discloses the anisotropic behaviors of 2D materials and puts emphasis on the mechanical anisotropy of three distinct 2D materials, namely graphene, MoS_2 and Al alloy coating, representative of carbon, inorganic and metallic 2D crystalline materials. Except for the relatively low interlayer cohesive stress, the in-plane anisotropy of the former two materials classes is subjected primarily to the hexagonal structure of the unit cells of the graphene and MoS_2. The anisotropy of metallic thin films with high-density grain boundaries with preferential directionality, rendered by the non-equilibrium synthetic methods, results from both the conventional Taylor factor and the directionality of the grain boundaries. Despite 2D materials' wide spectrum of applications, such as electronics, energy devices, sensors, coating etc., the mechanical anisotropy could be critical for certain mechanical applications, such as friction, and provide instructions on the durability, reliability and property optimization in the various applications of different 2D materials.

Keywords: anisotropy, mechanical behaviors, 2D materials, metallic materials, non-metallic materials
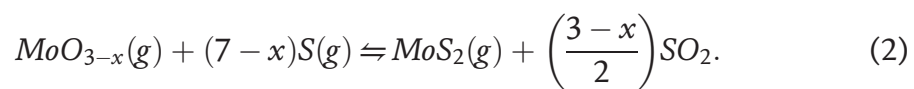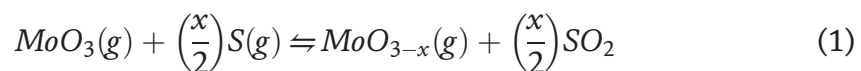
1. Introduction

As time passes, the advancement of nanotechnology has spread to all fronts. The concept states that at least two dimensions that construct nanomaterials fall between 1 and 100 nm. Nanomaterials are classified as zero- (0D), one- (1D), two- (2D), and three-dimensional (3D) nanostructures. The nanoscale has unprecedented attributes that fundamentally alter materials' properties. Since K. Novoselov et al. successfully mechanically exfoliated a single layer of graphene off the graphite in 2004 [1], extensive efforts and progress have been made on the synthesis and applications of graphene and various 2D nanomaterials in resemblance to graphene nanostructure, including transition metal dichalcogenides (TMDs), hexagonal boron nitride (BN), and perovskites, just to name a few. They have lateral extension but their individual layer is merely a single or few atoms thick. Hence, they have characteristics like electron confinement and anisotropy in various properties

manifested in two dimensions, while they possess extended interlayer spacing for active kinetic and physicochemical events, which has attracted broad research interests on their physicochemical, electrochemical, electronic and mechanical properties. For metallic materials, metallic thin films/coatings have 2D extension but limited thickness. The 2D materials selected to represent each materials family are crystalline materials and, in general, possess crystal anisotropy in their mechanical behaviors and even functional property. The single crystal face-centered cubic (FCC) structure is taken as an example. It is well known that the FCC single crystals have crystal anisotropy determined by the Schmid factor that associates the loading direction to the load resolved on the specific slip system [2]. Because the glide of the dislocations is favored on the slip systems subjected to a larger Schmid factor, plastic anisotropy manifests in the form of different cellular substructure made of dislocation walls. As we alleged, the non-metallic 2D nanomaterials have extended interlayer spacing and metallic thin films, fabricated primarily by ultrahigh vacuum techniques and electrodeposition, feature high-density directional grain boundaries (GBs) and preferential texture. As a result, anisotropy in 2D materials is prone to deviate from that of the bulk crystals, and plays substantial roles in their mechanical applications and the reliability of the apparatuses and devices with 2D materials as components or building blocks, but has not been put emphasis on as much as their functional properties and synthesis. Prior to comprehension toward the mechanical anisotropy of 2D materials, their general microstructural features and applications are first set forth so as to better grasp the anisotropy in their mechanical response to external stimuli and its importance in their functional and engineering applications.

1.1 The general microstructural features and applications of 2D materials

1.1.1 Non-metallic 2D materials

Graphene is a typical 2D carbon allotrope and a monolayer of graphene, with a thickness of 0.335 nm, has a hexagonal honeycomb structure. This 2D nanomaterial is remarkably electric and thermal conductive and is equipped with the promising quantum Hall effect. Moreover, the pristine graphene possesses an elastic modulus of ~1 TPa and a mechanical quality factor of 10^4 at an elevated temperature of 5 K. Despite similar sheet-like nanostructures, 2D nanomaterials made of inorganic compounds can render intriguing properties and versatility due to their more complex compositions. In contrary to chemically inert graphene with no intrinsic bandgap, MoS_2 with layered structure is one transition metal dichalcogenide. MoS_2 has been often synthesized using chemical vapor deposition (CVD) and its reaction principle involves first the transformation of solid-state MoO_3 and sublimed surfur to gas state and then the mixed gases driven by argon caused the formation of gas-phase MoO_{3-x} and MoS_2 and eventually the formation of solid-state MoS_2, the reactions of which is expressed as [3]:

$$MoO_3(g) + \left(\frac{x}{2}\right)S(g) \rightleftharpoons MoO_{3-x}(g) + \left(\frac{x}{2}\right)SO_2 \qquad (1)$$

$$MoO_{3-x}(g) + (7-x)S(g) \rightleftharpoons MoS_2(g) + \left(\frac{3-x}{2}\right)SO_2. \qquad (2)$$

MoS_2 structure is comprised of two layers of closely packed S atoms layers sandwiching a layer of Mo atoms and it features strong covalent bonding as a result of the Mo-S interaction and the Van der Waals force between S layers. This leads to the comparably facile kinetic transportation of ions and even molecules through

S-Mo-S layered structure [4]. Hence, it has drawn enormous attention for its potent applications in energy storage and conversion, such as photocatalysis for the pollutant degradation and biosensors, just to name a few. In addition, MoS_2 has a good tunability toward its band gap, which offers high flexibility in property customization and optimization. At the same time, MoS_2 manifests comparable physical attributes when compared to graphene, including high charge carrier mobility and superb wear properties. Compared to hexagonal structure, other structurally complex 2D materials, such as arsenic trisulfide (As_2S_3), also showed mechanical anisotropy [5]. A unit cell of As_2S_3 consists of two layers inverted with respect to a symmetry center and is defined by 20 atoms in contrast to two for graphene and three for MoS_2.

1.1.2 Metallic thin films

Now, we turn our attention to a different 2D materials family, i.e. metallic coating and thin films. The protective coatings, from an engineering point of view, are essential as to apparatus maintenance and the enhanced equipment safety and lifespan. One application of metallic or their composite coating is to prevent corrosion. Coatings should render compatibility with parental materials and operate at extreme atmospheres, such as high temperature and corrosive conditions. Metallic coatings either provide passive protection by forming a barrier of oxides or offer active protection obtained through the adsorption of chemical inhibitors [6]. Metallic coatings as biomaterials are potent components in body implants and they ought to possess superb mechanical behaviors and biocompatibility, and high corrosion resistance, while they are required to release minimal metallic ions to avoid the toxicity. Ti, NiTi, Pt and 316 L austenitic stainless steel are often implemented. Furthermore, various metals with unique characteristics are used in the applications of thin film optics, such as surface plasmon generation and optoelectronics. Metallic thin films are frequently applied onto ceramic matrices, rendering high-quality broadband reflective finishing highly desired to control over the directionality of the laser beam. In addition, Cu is commonly utilized as an interconnect material and serves as thin conductive layers ensuring the adhesion to dielectrics and inhibiting diffusion into silicon or dielectrics, and provide capability of electrodeposition of Cu [7]. From the aforementioned applications of metallic coating and thin films, it is realized that their fabrication often relies on non-equilibrium routes, such as a variety of ultrahigh vacuum techniques and electrodeposition/electroplating. The energetic adatoms landing on the substrate often first form nanometric epitaxial zone and then become 3D clusters during the growth process [8]. Moreover, the sophisticated compositions or the interaction between matrix atoms and impurity atoms as dopants and alloying elements often exert pinning effects. These factors result in the formation of abundant GBs among the columnar nanograins. Many thin films have been grown homo- or heteroepitaxially on single crystal templates or locally on polycrystalline templates, giving rise to the preferential texture in the films. Both the GB directionality and the preferential texture in the coatings or thin films should lead to mechanical and crystal anisotropies which greatly affect their performance in practical applications and hint at the property optimization along each direction.

1.2 Basics of anisotropy

In FCC single crystals, the Schmid factors mainly explains the crystal anisotropy. For a given crystal, different loading directions result in different sets of Schmid factors on the 24 slip systems FCC structure intrinsically has, eventually tailoring

dislocations on different slip systems. Along with the dislocation populations, the dislocations would self-organize into certain low energy substructures with cellular shape. For instance, [111]-loading generally leads to planar-shaped cell substructures, whereas [100] direction renders spherical-shaped ones. To be specific, the Schmid factors of the four slip planes for three different loading directions are present in **Table 1**. Z. Q. Wang et al. introduced an H-factor based on Schmid factors to comprehend the deformation heterogeneity and the formula is expressed as [2].

$$H = \frac{\tilde{m}_{i,max} - \tilde{m}_{i,min}}{\sum_i \tilde{m}_i} \tag{3}$$

where $\tilde{m}_i$ is the sum of all three values of the Schmid factors for each slip plane under one loading orientation, and $\tilde{m}_{i,max}$ and $\tilde{m}_{i,min}$ are the maximum and minimum of $\tilde{m}_i$ out of four different planes, respectively. This causes the $[\bar{2}11]$-, [111]- and [100]-loadings to render the respective H-factor of 0.376, 0.333 and 0. Moreover, this suggests that $[\bar{2}11]$-loading brings about highest flow stress and most heterogeneous cellular structure, where [100]-loading the lowest flow stress and most homogeneous structure out of three loading conditions.

For polycrystalline cubic metallic materials, the Yield strength is associated to a Taylor factor, M, based on the critical resolved shear stress (CRSS) and the Taylor factor relies on the active slip systems at the grain level of a polycrystalline metal with crystallographic preferential texture in the aggregate. According to the classic dislocation mechanics [9], the Yield strength can be defined as

$$\Delta\sigma_y = M\left[\tau_0 + \left(\frac{\tau^* \mu b}{\pi(1-v)L}\right)^2\right] \tag{4}$$

where τ_0 and L are the lattice friction and the mean spacing between a dislocation source to obstacle, respectively. τ^* denotes the barrier shear stress for a single dislocation transmission across a GB and v, b and μ are the Poisson's ratio, Burgers vector and the shear modulus, respectively. The Taylor factor is intimately associated with the stacking fault energy (SFE) as well as the ratio, ξ, of CRSS for twinning and slip for FCC metals. Besides FCC structure, various crystalline materials are anisotropic. For example, various carbides hexagonal M_7C_3 (M = Fe, Cr, W, Mo) exhibited anisotropy and difference in chemical bonding along different crystallographic orientation determined the anisotropy and their elastic anisotropy could be further tailored by the different atomic arrangement controlled by multialloying [10]. Despite different mechanisms, some liquid crystals can be defined as the anisotropic fluids whose form is between the isotropic liquid and the anisotropic crystalline phase [11].

|	[100]-loading	[111]-loading	$[\bar{2}11]$-loading
(111)	0.41, 0.41, 0.0	0.0, 0.0, 0.0	0.0, 0.0, 0.0
(1$\bar{1}$1)	0.41, 0.41, 0.0	0.27, 0.27, 0.0	0.41, 0.27, 0.14
($\bar{1}\bar{1}$1)	0.41, 0.41, 0.0	0.27, 0.27, 0.0	0.41, 0.27, 0.14
($\bar{1}$11)	0.41, 0.41, 0.0	0.27, 0.27, 0.0	0.27, 0.27, 0.0

Table 1.
Schmid factors of the four slip systems for three different loading directions. Reconstructed from reference [2].

1.3 Anisotropy in non-metallic 2D nanomaterials

The 2D non-metallic materials display remarked structural anisotropy due to the large interlayer spacing and comparably low interlayer cohesion and interaction, which causes that a monolayer of graphene could be readily mechanically exfoliated and hexagonal MoS_2 (h-MoS_2) with lamellar structure can be used as a solid lubricant owing to its superlubricity causing the facile glide among MoS_2 nanosheets. However, in the in-plane direction, the assumption of mechanical isotropy in 2D materials is premature just based on the six-fold symmetry in their hexagonal lattice when the isotropy has been assumed for some estimations of the elastic behaviors in carbon nanotubes. Prior researches unveiled that friction force exerted on both graphene and MoS_2 along in-plane 'zigzag' and 'armchair' directions of the hexagonal lattice gave rise to different results and friction tests along armchair direction resulted in larger friction forces. M. Dienwiebel et al. found the angular interval between two friction peak force being approximate 60° upon friction tests on graphite [12]. This suggests that the 2D materials with hexagonal lattice manifest a sixfold anisotropy with a 60° periodicity. Meanwhile, studies showed that the anisotropy in both graphene and MoS_2 has a thickness dependence [13]. 2D non-metallic nanomaterials have been often used as building blocks or components for micro/nano-electromechanical systems (M/NEMSs) and nanoelectronics. The anisotropy of those 2D materials have great influence on not only mechanical properties but also functional properties.

1.4 Anisotropy in metallic 2D thin films

Metallic coating and thin films have been largely fabricated adopting non-equilibrium ultrahigh vacuum techniques and electrodeposition. When the nuclei heterogeneously grow and then 3D clusters collide amid the coalescence process, forming intercrystalline interface. This process generally gives rise to nanocolumnar grains whose grain size is small, even in monolithic metals, in contrast to other equilibrium processes. **Figure 1** shows the structure zone diagram after energetic deposition of a thin film on a substrate, indicating that columnar grains preferentially being generated at different generalized temperature T/T_m and argon pressure [14]. The columnar structure could even exist in amorphous Al-Cr thin films prepared by the sputtering technique as a result of chemical segregation [15]. These 2D
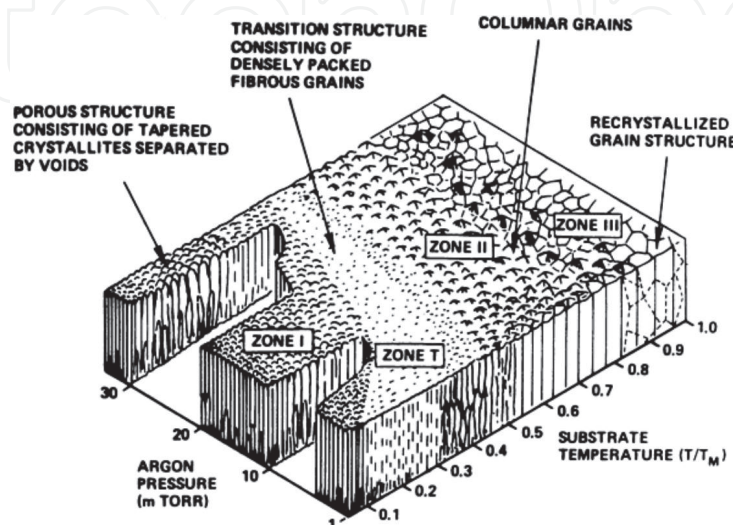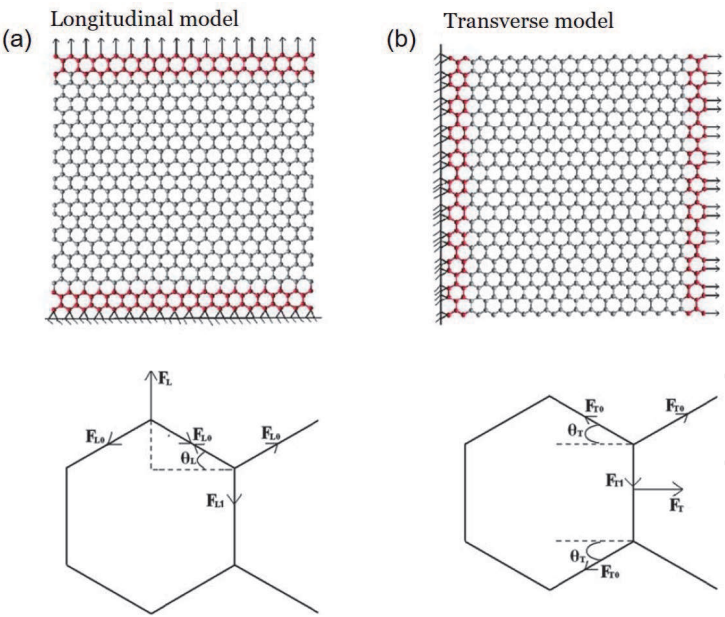

Figure 1.
Structure zone diagram after energetic deposition at different generalized temperature T/T_m *and argon pressure. Reprinted with permission from reference [14].*

metal coatings or thin films have higher hardness and strength, abiding by the well-known Hall–Petch relationship. However, the abundant columnar GBs with directionality are often the sites where the voids reside. The sluggish adatom kinetics and the shadowing effect from the surface e roughness lead to void formation residing at the columnar GBs and void-free GBs have lower cohesive energy when compared to the grain interiors. Z. S. You et al. found that nanotwinned (NT) Cu with columnar grains packed with horizontal coherent twin boundaries (TBs) experienced inhomogeneous deformation and columnar GBs were subjected to much larger plastic strain, compared to the grain interiors [16]. This caused one ambiguous puzzle, that is, the constant in the Tabor equation expressed as $H = C\sigma$ which translates the indentation hardness to the tensile strength often remarkably fails to fall in the proper proportionality range [9]. The proportionality constant, C, is dependent on the deformation mode under indentation and it had been empirically determined that H/$\sigma \approx$2.7 for materials with high strain hardening coefficient and yield strength (elastic–plastic transition mode). This indicates the 2D metallic thin films with columnar GBs possess substantial structural anisotropy, despite the crystal anisotropy governed by either Schmid factor or Taylor factor [2, 8]. Metallic coatings or thin films have been used as protective, reflective, conductive components on apparatuses and devices. Comprehension toward the anisotropy of 2D metallic materials would substantially help improve their reliability and realize property optimization.

## 2. Fraction anisotropy in graphene

It has been known that graphene, graphene oxide and their composites exhibit mechanical anisotropy due to their characteristic of 2D extension [17, 18]. The investigations on the superlubricity of 2D nanomaterials have been also extensively conducted. A classic example is that M. Dienwiebel et al. studied the energy dissipation of a graphite at selective sliding directions on a Tribolever setup equipped with a tungsten tip and found the ultralow friction with the incommensurability nature [12]. Another example is M. Poot and H. S. J. Van der Zant adopted atomic force microscope (AFM) to measure force-distance relations on few-layer graphene and graphite flakes and discovered that a principle direction represents a stiffer direction than the others [19]. In contrast to those studies, a molecular dynamics simulation (MD) study is particularly selected to exhibit the anisotropic mechanical behaviors of graphene monolayers under uniaxial tensile condition along the zigzag and armchair directions [11]. 4.15 × 4.15 nm^2 square-shaped graphene monolayers with a thickness of 0.335 nm were fixed at one end and the tensile tests along the zigzag and armchair directions are present in **Figure 2a** and **b**. The relations between applied force and one unit cell are also present. The specific parameters of the non-equilibrium MD simulations can be found in the literature.

Regardless of the fracture patterns, the MD experiments first calculated the fracture stresses along the zigzag and armchair directions, which are 0.18 TPa at a strain of 32.48% and 0.21 TPa at 43.85%, respectively. In is worth noting that the predicted critical stresses and strains are anticipated to be higher than the empirical ones due to the idealism in the conditions of MD simulations. Prior to the crack formation, two test modes share similarity, that is, in the elastic region, the graphene monolayers regardless of testing directions could sustain large elastic deformation and upon crack formations, the crack propagated rapidly and led to the final fracture within 0.01% strain, suggestive of a brittle cleavage fracture. For the zigzag direction, within the strain from 32.484% to 32.489%, the crack propagated from one edge to the other edge, forming a zigzag-like fracture topography and the

Figure 2.
Molecular dynamics simulation of tensile tests on 4.15 × 4.15 nm² square-shaped graphene monolayer along (a) zigzag and (b) armchair directions and the relations between applied force and one unit cell are present. Reprinted with permission from reference [20].

topological defects, whereas a rather smooth fracture feature was monitored as the strain varied from 43.859% to 43.866% under the test along armchair direction and the process left limited topological defects. It should be noted the five significant digits might be trivial in the real experiments but it was non-trivial in the MD simulations to capture detailed fracture process. The fracture evolutions along two directions were captured using snapshots in **Figure 3**. Since the C-C bonds have a critical strength, i.e. σ_{C-C}, it is anticipated that the direction of the applied force with respect to the hexagonal honeycomb lattice eventually governed the fracture mode and the analysis on the evolution of bond angles during the straining under two testing conditions is essential to decipher the different fracture mechanisms. Along the ziazag direction in **Figure 3a**, two 120° bond angles that evolved in a symmetrical pattern with the increase in the strain declined down to <90 ° and sustained substantial external strain, while the bonds in parallel to the tensile
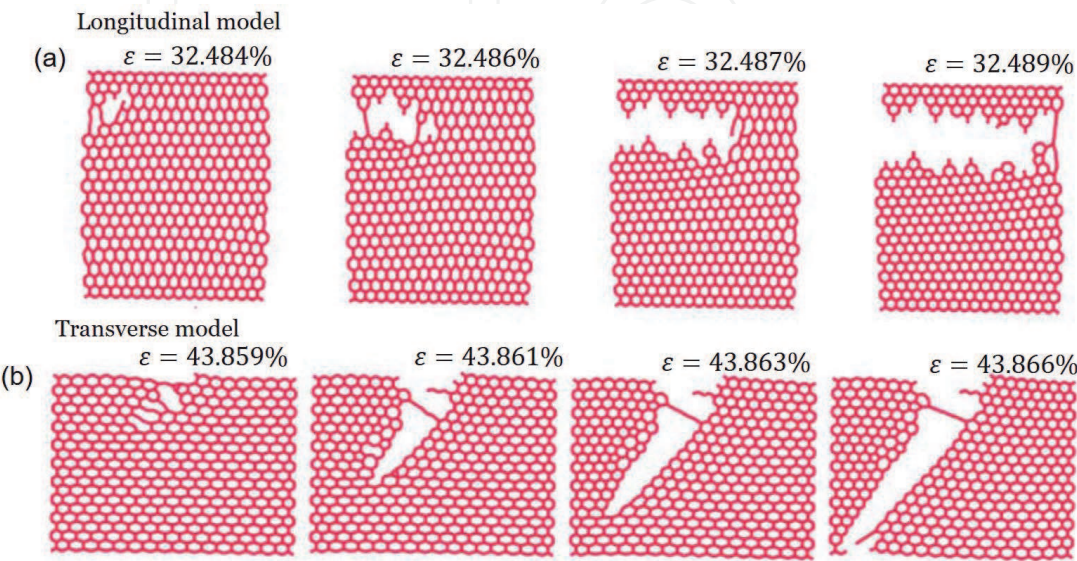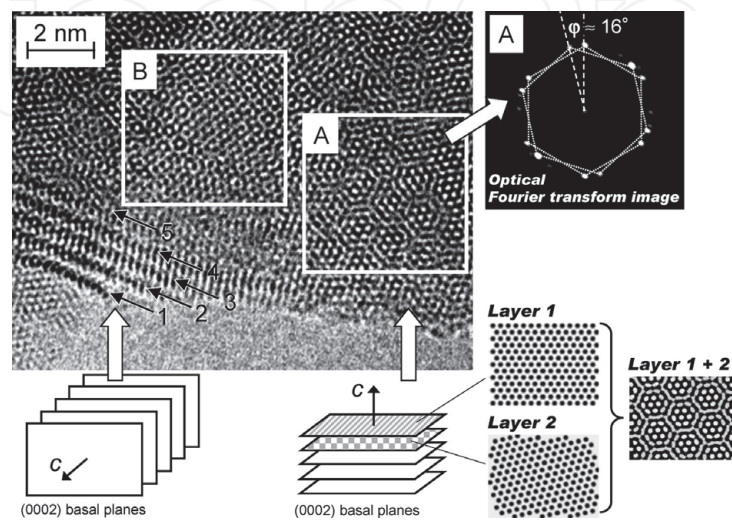

Figure 3.
Tensile strain-induced fracture process (a) along the zigzag direction and (b) along the armchair direction at various strain levels. Reprinted with permission from reference [20].

direction were elastically deformed until their critical strength was reached and then they broke, forming the broken hanging chains. In the other hand, the deformation along the armchair direction in **Figure 3b** caused the four 120° bond angles with a ± 30 ° relation with the applied force to decrease, transferring the hexagonal lattice into the quasi-rectangular shape, until any of the bonds except the two bonds normal to the testing direction broke. In the armchair mode, once triggered, the crack front would lead to a sequential instantaneous bond-breaking along the same direction and this left a 60° rupture along the armchair direction. Therefore, the two bonds parallel to the zigzag testing direction and the four bonds perpendicular to the armchair testing directions underwent the larger stress. As a result, the critical stress along the armchair is calculated to be $\sqrt{3}\sigma_{C-C}$, 1.73 times of the σ_{C-C} of the zigzag direction. In reality, the 0.21 TPa of the armchair direction is approximately 1.2 times of the 0.18 TPa of the ziazag direction, which is attributed to the evolving geometrical changes of the hexagonal structures amid the elongation processes. In addition, the geometrical changes of the hexagonal units during the straining determined the critical fracture stains for two testing directions. In order to validate the observation, the simulated dimensions were investigated to verify if the mechanical anisotropy has a size effect and it was found that the size effect was negligible.

3. Friction anisotropy in MoS2

The MoS_2 has similar lamellar structure as graphene and has been considered promising in the field of nanotribology, despite its various applications due to its functional properties. The inherent crystallographic characteristics of h-MoS_2 equips it with friction anisotropy pertaining to the effect of the lateral sliding direction on the friction behaviors or the commensurability/incommensurability conditions between two sliding planes. In the case of incommensurability where the two sliding surfaces have crystallographic nonmatching, ultralow friction is obtained and superlubricity occurs, which has been observed in 2D materials, such as MoS_2, graphene and highly oriented pyrolytic graphite to name a few. The superlubricity is related to the structural anisotropy. **Figure 4** presents the debris of five-layer thick MoS_2 after a wear test and the high resolution transition electron
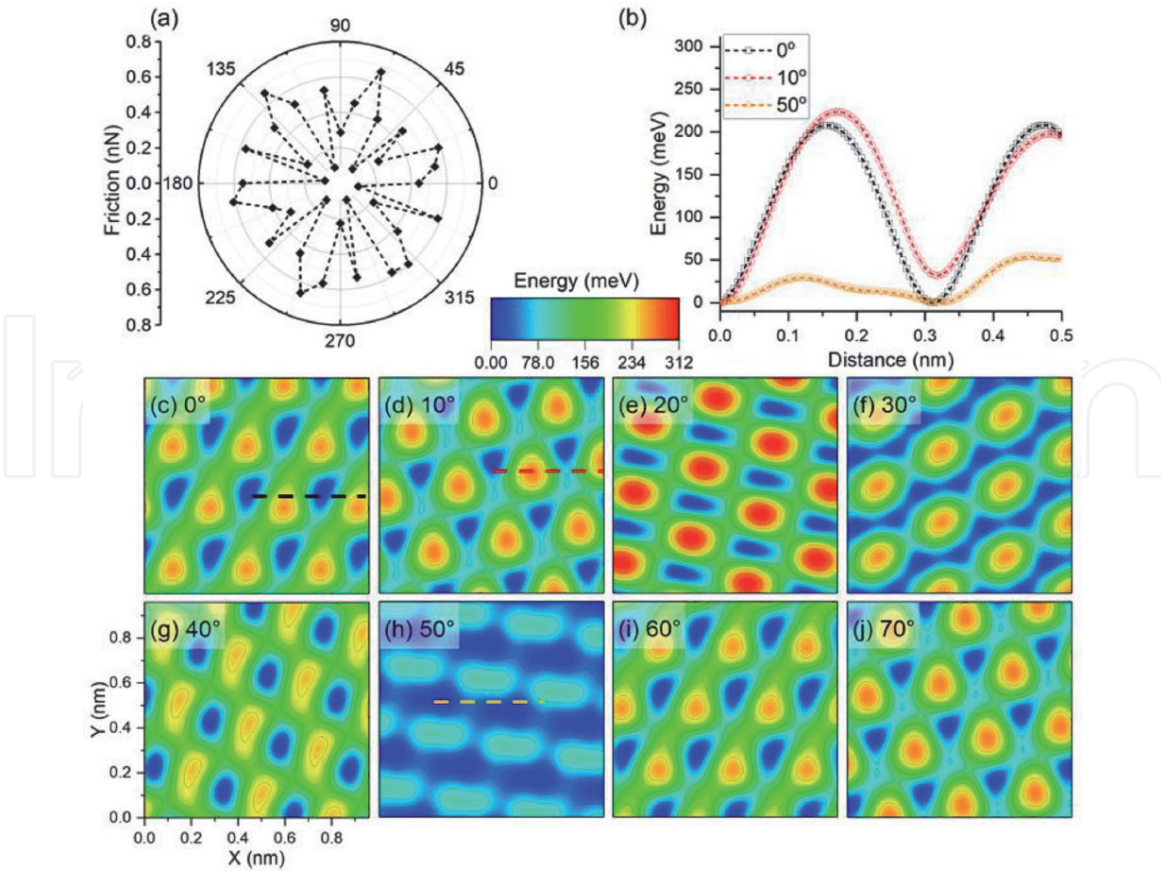

Figure 4.
High resolution TEM micrograph of a five-layer thick MoS₂ specimen after a wear test and the slide led to different mosaic lattice domains with 15° and 30° relative rotations. Reprinted with permission from reference [21].

microscopic (HRTEM) image shows different mosaic lattice domains as a result of 15° and 30° relative rotations between MoS_2 nanosheets [21]. Commonly, six-fold and two-fold symmetry of the friction behaviors have been captured on empirical and computational researches. Some two-fold symmetry of friction behaviors, namely 180° periodicity, have been attributed to the oriented linear wrinkles induced by the elastic deformation of the substrate and the testing conditions, one of which is the direction-dependent friction measured by an AFM tip with rotation. It was hypothesized that the tip rotation generated a variety of possible combination of the tip-specimen interfaces and the friction results might be able to reflect the genuine crystallographic pattern of the tested materials.

A study involving experimental and MD simulation results on the friction property of MoS_2 was present [22]. The direction-dependent friction behaviors were measured by changing the scanning direction and a 5 nm travel distance was applied to preclude the influence from the nanowrinkles. The atomic configuration and the scanning direction with respect to the lattice are illustrated in **Figure 5a**. **Figure 5b** presents the two friction loops consisting of forward and backward lateral scans, measured by AFM along zigzag and armchair directions, and it shows that the energy dissipated in each scan cycle of the tests along the armchair direction was 11 times higher than that of the tests along the zigzag direction. **Figure 5c** shows comparable simulation results and the quantitative discrepancy between the empirical and simulation results originates from the difference in tip conditions and the magnitude of the scanning speed and force. The Prandtl-Tomlinson model alleged that the friction at the atomic level relies on the height of the surface energy barrier and longer scanning length along the armchair direction would result in accumulated energy dissipation in comparison with the zigzag direction. Hence, the direction-dependent friction behaviors were examined using potential energy surface (PES). **Figure 6a** reveals a six-fold symmetry of the friction force in nN in comparison with the two-fold symmetry. To further comprehend the friction symmetry, PEC at various angular positions was observed with a 10° interval. **Figure 6b** reflects the cross-section energy profiles for the scans at 0°, 10° and 50°. **Figure 6c-j** show that PES possessed a 60° periodicity, e.g. the energy surfaces of the 0° and 60° being identical. Therefore, a friction anisotropy was explored at an atomic level, proving that the testing direction and tip-specimen contact quality greatly play significant roles in changing the energy landscape and affecting the friction behaviors. X. Cao et al. have exhibited that the friction behaviors of MoS_2 had a thickness effect [13]. In brief, the decrease in MoS_2 thickness down to a few nanometers could progressively weaken the anisotropy phenomenon and be more governed by the puckering effect.
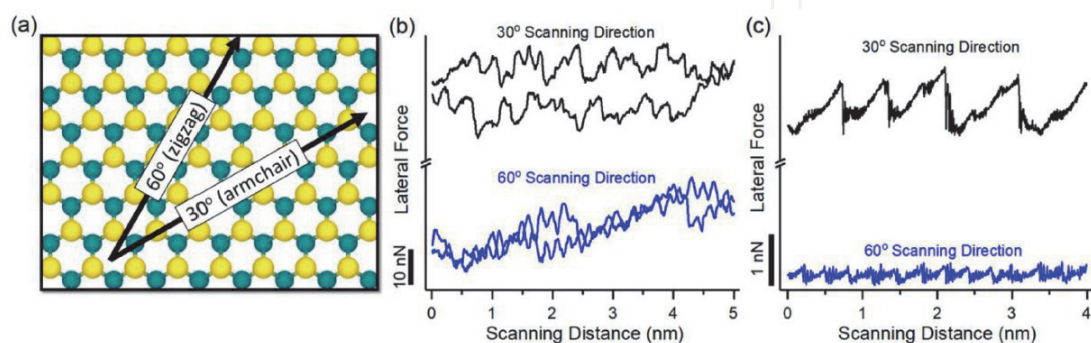
Figure 5.
(a) Atomic configuration of a MoS_2 monolayer in the simulations, indicating the armchair (30°) and zigzag directions (60°). (b) the experimental friction loops consisting of the forward and backward scanning along the armchair and zigzag directions. (c) the friction traces, due to tip-specimen contacts, predicted by the MD simulations along the armchair and zigzag directions. Reprinted with permission from reference [22].

Figure 6.
(a) MD simulation that monitored a 6-fold symmetry in the results of friction tests on MoS₂ as a function of the rotational. (b) Cross-sectional barrier profiles along the scanning distance at a sample rotation angle of 0°, 10° and 50°. (c − j) potential energy surface (PES) calculated for the specimen rotated from 0° to 70°. Reprinted with permission from reference [22].

4. Mechanical anisotropy in Al-Fe thin films

Since the early 1950's when Hall and Petch empirically demonstrated that the Yield strength of metallic materials is inversely proportional to the square root of the microstructural features, researchers have put enormous efforts in refining the microstructure and thus developed ultrafine grained materials and nanocrystalline materials in order to lift mechanical strength for both fundamental exploration and practical applications. Non-equilibrium routes have been commonly used to shrink the grain size of the metallic materials and most of techniques, such as ultrahigh vacuum techniques and electrodeposition, produce 2D metallic materials, i.e. coatings and thin films. Researchers have found that the tensile strength collected from the tensile tests on thin film metals, especially alloys, fell short of the predicted strength translated from nanoindentation measurements according to the Taylor relation, i.e. H = Cσ where C is the proportionality constant. H/σ = 3 is often observed for materials with low strain hardening coefficient and low yield strength (fully plastic contact mode), whereas 1.1 < H/σ < 3 is applicable for materials with high strain hardening coefficient and high yield strength (elastic–plastic transition mode). Most of time, nanoindentation studies showed empirically that H/σ≈2.7 for thin film metals with high strength. The off-proportionality has been often attributed to the voids potentially residing at the columnar GBs in thin film materials. However, the void size is proportional to columnar grain size and when the grain size is at nanoscale, the shadowing effect that originates from the 3D cluster growth should be negligible to cause void formation. Therefore, the directionality of the

columnar GBs that contributes to the structural anisotropy has been largely ignored. Li et al. selected Al-Fe alloys produced by magnetron sputtering to investigate the anisotropy and tension-compression asymmetry along both the film in-plane and out-of-plane directions by adopting comprehensive in-situ micro-compression and tension techniques [9].

Figure 7a shows the dark-field TEM image and HRTEM image, suggesting that the Al-Fe alloys have abundant vertical GBs, which were identified as incoherent twin boundaries (ITBs) with a diffused feature, and an average grain size of ~5 nm. It is expected that the tiny grain size would greatly suppress the dislocation accumulation process that takes place in the plastic deformation of single crystals or polycrystalline materials with large grain size, making the deformation or fracture events more dominantly influenced by the directionality of the GBs. **Figure 7b-d** illustrate the micro-tension and compression experiments along in-plane and out-of-plane directions and exhibit the microsized specimens awaiting the in-situ experiments.

The experiment results showed that the out-of-plane compression experiments gave rise to a ~ 2 GPa strength and exhibited extensive deformability attributed to the grain coarsening, whereas in-plane compressions yielded a ~ 1.6 GPa strength but an intergranular shear deformation along the GBs, leaving the formation of shear bands. This deformation mode was governed by the maximum resolved shear stress. In addition, out-of-plane tensile experiments gave a tensile strength of ~1.8 GPa, comparable to the 2 GPa compressive strength, and a fracture mode governed by the intragranular shear propagation which were substantially deflected by vertical GBs. The apparent global engineering strain cannot be equated to the
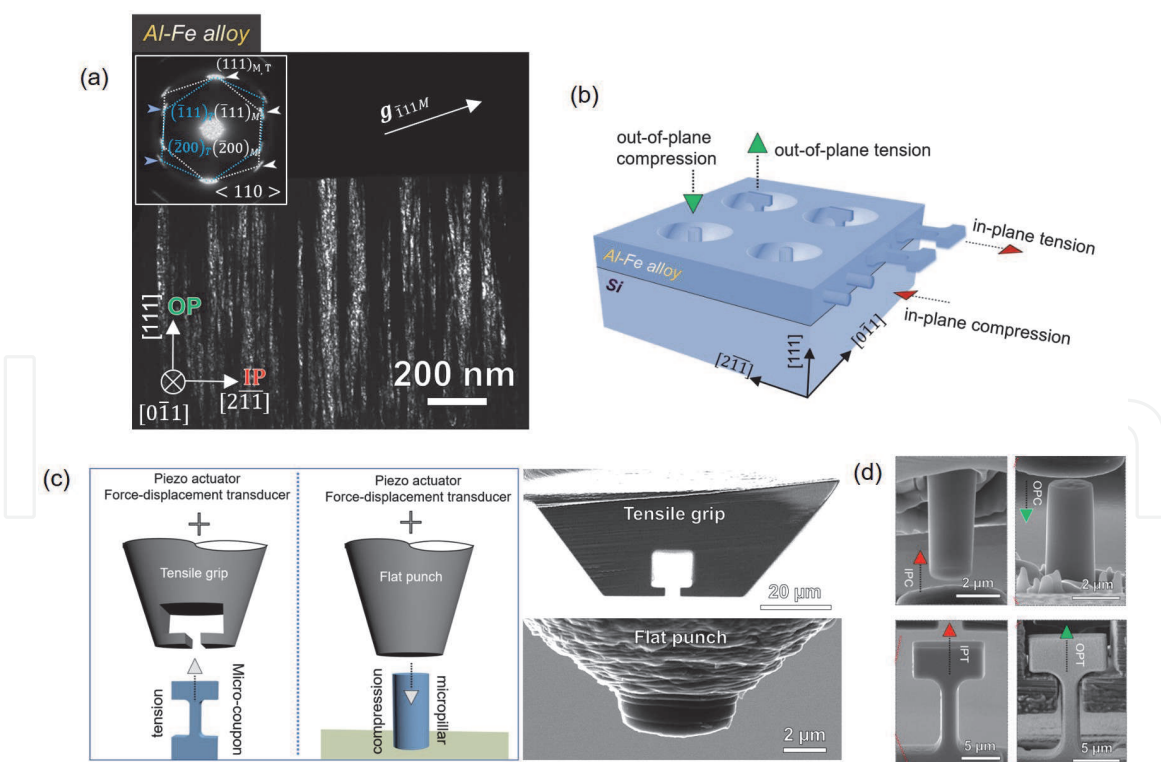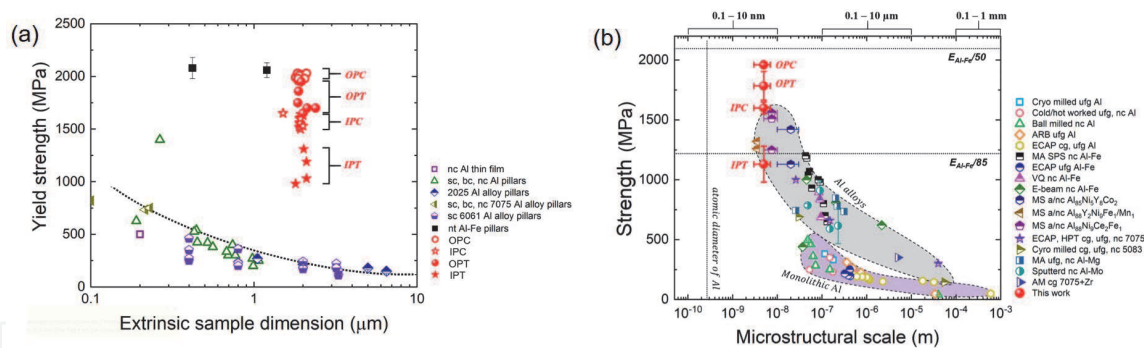

Figure 7.
(a) Cross-section dark-field TEM image showing abundant vertical GBs in a (111)-textured Al-Fe thin film and the neighboring columnar nanograins having twin relation. (b) Schematics illustrating how to perform micro-tension and compression experiments along both in-plane and out-of-plane directions. (c) Schematics of the setups of the in-situ *micro-tension and compression experiments along with the scanning electron microscope (SEM) images of the tensile gripper and the flat punch. (d) Micropillars and tensile micro-coupons awaiting the in-situ tension and compression experiments. Note that OPC, IPC, OPT and IPT denote out-of-plane compression, in-plane compression, out-of-plane tension, and in-plane tension, respectively. Reprinted with permission from reference [9].*

ductility of the common ductile materials with larger grain size and dislocation-dominated deformation mechanisms. In contrast, the in-plane tension experiments exhibited a relatively low strength of ~1.1 GPa and classic brittle behaviors governed by the nominal stress-induced fracture. The premature fracture propagated along GBs. It was found that the chemical combination of binary Al-Fe alloys did not satisfy the embrittlement criteria in the Gibson-Schuh model [23], meaning that the relation between applied tensile stress and the directionality of the vertical void-free GBs, i.e. vertical ITBs, mostly rendered the premature fracture phenomenon under in-plane tension mode rather than other factors including voids and GB embrittlement. **Figure 8** had summarized the major deformation or fracture mechanisms of the tension and compression tests along the in-plane and out-of-plane directions. It is noted that the anisotropy experienced in the Al-Fe thin films is different from the anisotropy in single crystals and polycrystals, governed by the Schmid factor and the Tylor factors. Moreover, the thin film alloys, including the Al-Fe, are also different from the isotropic nanocrystalline metals and alloys with textureless feature. However, dislocations were indeed captured in the differently deformed Al-Fe specimens. It was found that under compression, the ratio of the yield strength collected under out-of-plane compression mode and in-plane compression mode was ~1.25, which was mostly governed by the Taylor factors of two testing directions. Since the Al-Fe alloys have a strong (111) out-of-plane texture, the out-of-plane Taylor factor is 3.67. Moreover, the in-plane direction has no obvious texture or a weak (112) texture and the two possibilities rendered similar Taylor factor of 3.06. This two Taylor factors led to a strength ratio of 1.2, coinciding with the 1.25 collected experimentally. This indicates that the anisotropy in the Al-Fe thin films was both influenced by the directionality of the GBs and the
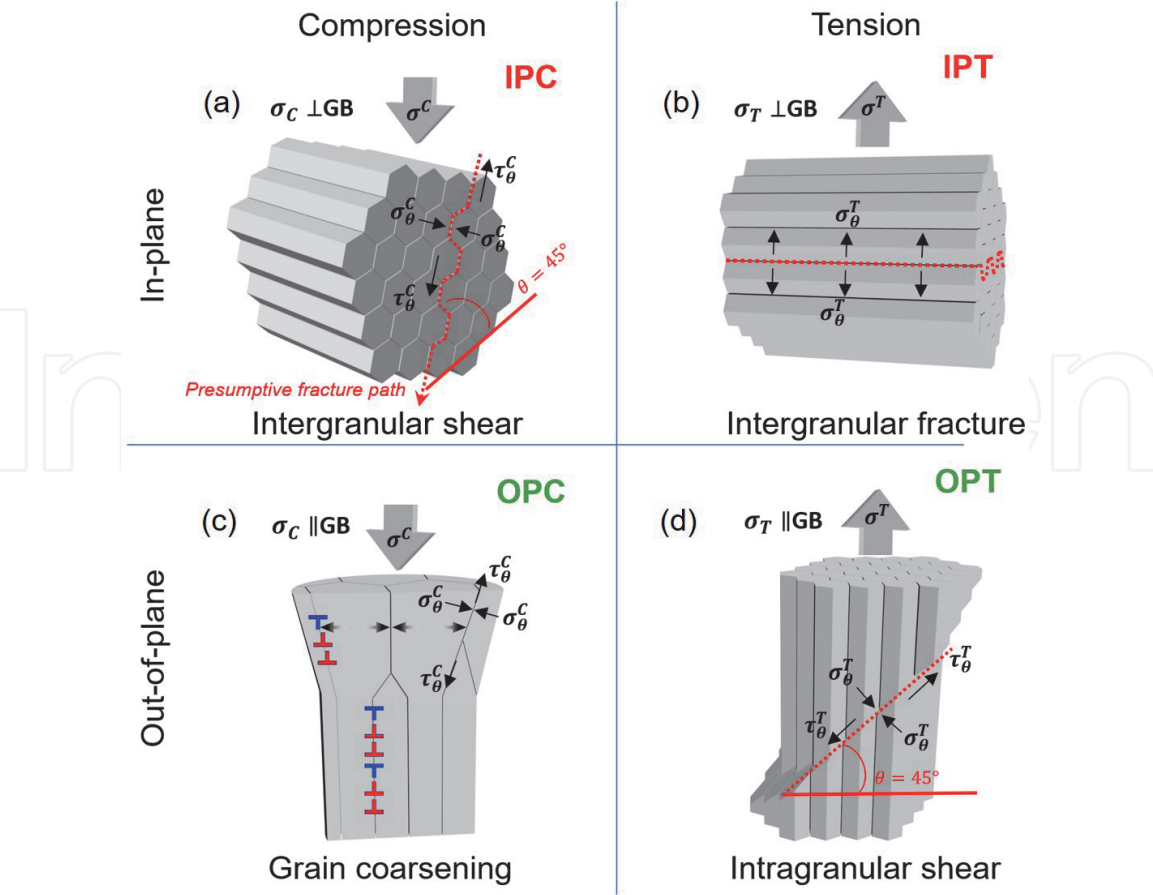
Figure 8.
Schematics that illustrate the deformation or fracture mechanisms for Al-Fe specimens tested at different modes along different directions. Reprinted with permission from reference [9].

Figure 9.
(a) The yield strength or fracture strength, collected from different testing conditions, of Al-Fe thin films in comparison to the ones of other Al alloys with extrinsic dimensions at similar magnitudes. (b) the comparison of the strengths as a function of intrinsic microstructural feature size effect between Al-Fe thin film and other pure Al and Al alloys. Reprinted with permission from reference [9].

conventional Taylor factor. **Figure 9** plots the collected strengths under tension and compression along the in-plane and out-of-plane directions as a function of extrinsic specimen dimension and intrinsic microstructural feature size and it clearly manifested the anisotropy under both tension and compression modes. The Al-Fe alloys underwent negligible extrinsic size effect and are highly competitive as to the high strength.

Some thin films or coatings consisting of constituent elements with low stacking fault energy might have columnar grains packed with high-density horizontal coherent TBs (CTBs). Q. H. Lu et al. found that the dislocations were confined within the twin/matrix lamellae and the testing direction, the slip systems and the horizontal CTBs of the NT Cu could result in different dislocation structures and dislocation-CTB interactions, which rendered different hardening and softening modes and thus the anisotropy in metallic thin films made of constituent elements with low stacking fault energy [24]. Furthermore, it should be noted that not all the metallic thin films prepared by non-equilibrium methods possessed the conventional columnar GBs. Li et al. recently exhibited that manipulation of electrolytic solution with certain organic additive could potentially transfer the 3D cluster growth to a flat 2D layer-by-layer growth mode to facilitate the formation of TBs and suppress the formation of the columnar GBs from the island coalescence process [8]. The anisotropy of the NT metals mainly constructed by horizontal CTBs needs further investigation. Furthermore, the mechanical anisotropy in metallic materials could be also displayed from the dynamic strain-induced phase transformation. In a Transformation induced plasticity (TRIP) steel, a strong texture after rolling was obtained in the austenite and the texture in austenite gave rise to a higher martensitic transformation rate along the rolling direction, which contributed to a more pronounced TRIP effect and a higher strain-hardening rate [25, 26].

5. Conclusions

The synthesis, microstructural controls and the functional applications of 2D materials have been top trending research topics in the past 2 decades. However, the anisotropy of the 2D materials has not been put equal but actually exerts potent influence on not only their mechanical behaviors but also the multifunctional performance of materials and devices with 2D materials as components or building blocks. The unique microstructural characteristics of 2D materials result in distinct and intriguing structural and crystal anisotropy. As to the non-metallic 2D nanomaterials, such as graphene and MoS_2, the orientation of the applied stress

with respect to the lattice often cause different interlayer friction, even the superlubricity, and the monolayer with the inherent crystallographic symmetry of the hexagonal honeycomb lattice also exhibited anisotropy when subjected to fracture. For the metallic thin films with 2D extension and limited thickness, the directional and abundant grain boundaries could influence the anisotropy comparison with the bulk single crystals or polycrystals whose anisotropy is primarily dominated by the Schmid factor or Taylor factor. It is anticipated that the sustainability and reliability of the materials and devices constructed by various 2D materials rely on the prominent anisotropy inside 2D materials. The in-depth comprehension toward the anisotropy of 2D materials would be also instructive to realize the orientation-dependent properties and the property optimization.

Author details

Qiang Li
School of Materials Engineering, Purdue University, West Lafayette, IN,
United States

*Address all correspondence to: qnli2015@gmail.com

IntechOpen

References

[1] Novoselov KS, Geim AK, Morozov SV, Jiang D, Zhang Y, Dubonos SV, Grigorieva IV, Firsov AA. Electric Field Effect in Atomically Thin Carbon Films. Science. 2004;306(5696): 666–669. DOI: 10.1126/science.1102896

[2] Wang ZQ, Beyerlein IJ, Lesar R. Plastic anisotropy in fcc single crystals in high rate deformation. Int. J. Plasticity. 2009;25:26–48. DOI: 10.1016/j.ijplas.2008.01.006

[3] Jian JY, Chang HL, Xu T. Structure and properties of single-layer MoS_2 for nano-photoelectric devices. Materials. 2019;12:198. ; Doi:10.3390/ma12020198

[4] Tan CL, Cao XH, Wu XJ, He QY, Yang J, Zhang X, Chen JZ, Zhao W, Han SK, Nam GH, Sindoro M, Zhang H. Recent Advances in Ultrathin Two-Dimensional Nanomaterials. Chem. Rev. (2017);117(9):6225–6331. DOI: 10.1021/acs.chemrev.6b00558

[5] Šiškins M, Lee M, Alijani F, Van Blankenstein MR, Davidovikj D, Van der Zant HSJ, Steeneken PG. Highly Anisotropic Mechanical and Optical Properties of 2D Layered As_2S_3 Membranes. ACS Nano. 2019;13(9): 10845–10851. DOI: 10.1021/acsnano.9b06161

[6] Moreno FP, Jakab MA, Tailleart N, Goldman M, Scully JR. Corrosion-resistant metallic coatings. Materials Today. 2008;11(10):14–23. DOI: 10.1016/S1369-7021(08)70203-7

[7] Hsiao HY, Liu CM, Lin HW, Liu TC, Lu CL, Huang YS, Chen C, Tu KN. Unidirectional Growth of Microbumps on (111)-Oriented and Nanotwinned Copper. Science. 2012;336(6084):1007–1010. DOI: 10.1126/science.1216511

[8] Li Q, Xue SC, Price P, Sun X, Ding J, Shang ZX, Fan Z, Wang H, Zhang Y, Chen YX, Wang HY, Hattar K, Zhang XH. Hierarchical nanotwins in single-crystal-like nickel with high strength and corrosion resistance produced via a hybrid technique. Nanoscale. 2020;12:1356–1365. DOI: 10.1039/C9NR07472D

[9] Li Q, Xue SC, Zhang YF, Sun X, Wang HY, Zhang XH. Plastic anisotropy and tension-compression asymmetry in nanotwinned Al–Fe alloys: An *in-situ* micromechanical investigation. Int. J. Plasticity. 2020;132:102760. DOI: 10.1016/j.ijplas.2020.102760

[10] Chong XY, Hu MY, Shan Q, Jiang YH, Li ZL, Feng J. Tailoring the anisotropic mechanical properties of hexagonal M7X3 (M=Fe, Cr, W, Mo; X= C, B) by multialloying. Acta Materialia. 2019;169:193–208. DOI: 10.1016/j.actamat.2019.03.015

[11] Asiya SI, Pal K, Kralj S, Thomas S. Nanomaterials dispersed liquid crystalline self-assembly of hybrid matrix application towards thermal sensor. Nanofabrication for Smart Na nosensor Applications. 2020:295–321. DOI: 10.1016/B978-0-12-820702-4.00013-1

[12] Dienwiebel M, Verhoeven GS, Pradeep N, Frenken JWM, Heimberg JA, Zandbergen HW. Superlubricity of graphite. Physical Review Letters. 2004; 92(12):12601. DOI: 10.1103/PhysRevLett.92.126101

[13] Cao XA, Gan XH, Lang HJ, Yu K, Ding SY, Peng YT, Yi WM. Anisotropic nanofriction on MoS_2 with different thicknesses. Tribology International. 2019;134:308–316. DOI: 10.1016/j.triboint.2019.02.010

[14] Thornton JA. Influence of apparatus geometry and deposition conditions on the structure and topography of thick sputtered coatings. Journal of Vacuum

Science and Technology. 1974;11:666–670. DOI: 10.1116/1.1312732

[15] Li Q, Shang ZX, Sun X, Fan CC, Su RZ, Richter NA, Fan Z, Zhang YF, Xue SC, Wang HY, Zhang XH. High-strength and tunable plasticity in sputtered Al–Cr alloys with multistage phase transformations. International Journal of Plasticity. 2021;137:102915. DOI: 10.1016/j.ijplas.2020.102915

[16] You ZS, Lu L, Lu K. Tensile behavior of columnar grained Cu with preferentially oriented nanoscale twins. Acta Materialia. 2011;59:6927–6937. DOI: 10.1016/j.actamat.2011.07.044

[17] Chu K, Wang F, Wang, XH, Huang DJ. Anisotropic mechanical properties of graphene/copper composites with aligned graphene. Materials Science and Engineering: A. 2018;713(24):269–277. DOI: 10.1016/j.msea.2017.12.080

[18] Jayan JS, Pal K, Saritha A, Seeraj BDS, Joseph K. Graphene oxide as multi-functional initiator and effective molecular reinforcement in PVP/epoxy composites. Journal of Molecular Structure. 2021;1230:129873. DOI: 10.1016/j.molstruc.2021.129873

[19] Poot M, Van der Zant HSJ. Nanomechanical properties of few-layer graphene membranes. Applied Physics Letters. 2008;92:063111. DOI: 10.1063/1.2857472

[20] Ni ZH, Bu H, Zou M, Yi H, Bi KD, Chen YF. Anisotropic mechanical properties of graphene sheets from molecular dynamics. Physica B. 2010; 405(5):1301–1306. DOI: 10.1016/j.physb.2009.11.071

[21] Onodera T, Morita Y, Nagumo R, Miura R, Suzuki A, Tsuboi H, Hatakeyama N, Endou A, Takaba H, Dassenoy F, Minfray C, Pottuz LJ, Kubo M, Martin JM, Miyamoto A. A Computational Chemistry Study on Friction of h-MoS$_2$. Part II. Friction Anisotropy. J. Phys. Chem. B. 2010;114: 15832–15838. DOI: 10.1021/jp1064775

[22] Vazirisereshk MR, Hasz K, Carpick RW, Martini A. Friction anisotropy of MoS$_2$: effects of tip-sample contact quality. J. Phys. Chem. Lett. 2020;11:6900–6906. DOI: 10.1021/acs.jpclett.0c01617

[23] Gibson MA, Schuh CA. Segregation-induced changes in grain boundary cohesion and embrittlement in binary alloys. Acta Materialia. 2015;95:145–155. DOI: 10.1016/j.actamat.2015.05.004

[24] Lu QH, You ZS, Huang XX, Hansen N, Lu L. Dependence of dislocation structure on orientation and slip systems in highly oriented nanotwinned Cu. Acta Mater. 2017;127: 85–97. DOI: 10.1016/j.actamat.2017.01.016

[25] Chen SC, Huang CY, Wang YT, Huang CY, Yen HW.Role of the crystallographic texture in anisotropic mechanical properties of a newly-developed hot-rolled TRIP steel. Materials Science and Engineering: A. 2020;790:139683. DOI: 10.1016/j.msea.2020.139683

[26] Min KM, Jeong W, Hong SH, Lee CA, Cha PR, Han HN, Lee MG. Integrated crystal plasticity and phase field model for prediction of recrystallization texture and anisotropic mechanical properties of cold-rolled ultra-low carbon steels. International Journal of Plasticity. 2020;127:102644. DOI: 10.1016/j.ijplas.2019.102644